STRUCTURAL CONTROL AND HEALTH MONITORING
Struct. Control Health Monit. 2017; 24: e1879
Published online 15 May 2016 in Wiley Online Library (wileyonlinelibrary.com). DOI: 10.1002/stc.1879

Assessing the effect of nonlinearities on the performance of a tuned inerter damper

Alicia Gonzalez-Buelga*,†, Irina F. Lazar, Jason Z. Jiang, Simon A. Neild and Daniel J. Inman

Department of Mechanical Engineering, University of Bristol, Queen's Building, University Walk, BS8 1TR Bristol, UK

SUMMARY

In this paper, the use of a tuned inerter damper (TID) as a vibration absorber is studied numerically and experimentally, with civil engineering applications in mind. Inerters complete the analogy between mechanical and electrical networks, as the mechanical element equivalent to a capacitor and were developed in the 2000s. Initially, inerters were used for applications in automotive engineering, where they are known as J-dampers. Recently, research has suggested that inerter-based networks could be used for civil engineering applications, offering interesting advantages over traditional tuned mass dampers. In the civil engineering context, research has been mainly theoretical, considering ideal inerters. Because the dynamics of an inerter device include nonlinearities, especially at the low frequencies associated with civil engineering applications, the performance of the TID device using an off-the-shelf inerter has been experimentally tested in the work presented here. The chosen system, comprising a host structure with a TID attached to it, was tested using real-time dynamic substructuring (RTDS) or hybrid testing. The inerter was tested physically, while the remaining components of the TID device, the spring and damper, together with the host structure, were simulated numerically. Displacements and forces at the interface between numerical and physical components are updated in real time. This numerical–physical split allows the optimisation of the TID parameters, because the values of the spring and the damper can be changed without altering the experimental setup. In addition, this configuration takes into account the inerter's potentially complex dynamics by testing it experimentally, together with the characteristics of the host structure. Developing RTDS tests for physical inertial substructures, where part of the fed back interface forces are proportional to acceleration, is a challenging task because of delays arising at the interface between the experimental and the numerical substructures. Problems associated with stability issues caused by delay and causality arise, because we are dealing with neutral and advanced delayed differential equations. A new approach for the substructuring algorithm is proposed, consisting of feeding back the measured force deviation from the ideal inerter instead of the actual force at the interface. The experimental results show that with appropriate retuning of the components in the TID device, the performance in the TID incorporating the real inerter device is close to the ideal inerter device. © 2016 The Authors. Structural Control and Health Monitoring published by John Wiley & Sons, Ltd.

Received 28 September 2015; Revised 7 March 2016; Accepted 20 April 2016

KEY WORDS: inerter; vibration suppression; substructuring; stability

1. INTRODUCTION

The inerter was developed by Smith [1] in the 2000s to complete the force–current electrical–mechanical analogy; an inerter is the equivalent to a capacitor in this analogy. The ideal inerter was defined as a mechanical two-node (two-terminal), one-port device with the property that the equal and opposite force applied at the nodes is proportional to the relative acceleration between the nodes [1]. Using the same analogy, a mass is the equivalent of a grounded capacitor, while the dampers

*Correspondence to: Alicia Gonzalez-Buelga, Department of Mechanical Engineering, University of Bristol, Queen's Building, University Walk, BS8 1TR Bristol, UK.
†E-mail: a.gonzalezbuelga@bristol.ac.uk

and springs represent the mechanical equivalents of resistors and inductors, respectively. A simple approach to synthesise an inerter is to have a rod sliding in linear bearings that drives a flywheel via a rack, pinion and gears [1]. There is also the possibility of building fluid inerters using the mass of a fluid flowing through a helical channel to provide the inertial force [2]. New inerter-based devices have been patented where, for example, variable intertance can be achieved by using a continuously variable transmission and gear-ratio control system [3]. In [4], an inerter was synthesised in the electrical domain, by using an electromagnetic transducer.

Since the invention of the inerter, it has been applied successfully in the automotive industry [5] and in the development of train suspensions [6,7]. Recent studies have looked into the use of inerters for civil engineering applications [8–12]. In [8], the tuned inerter damper (TID) was proposed to reduce vibrations in civil engineering structures subjected to base excitation. The numerical study concluded that the performance is comparable with or improves on that of a traditional tuned mass damper (TMD), with a number of important advantages such as smaller overall device size due to gearing and the capability to damp out high frequency responses away from resonance. The TID configuration is the network that will be studied in this paper and is depicted in Figure 1. Other inerter configurations have been proposed such as that presented in [9], which considers a traditional TMD, with an additional inerter in parallel with the spring and damper. This work concluded that with the incorporation of the inerter, lighter devices can be achieved, when compared with traditional TMD, while maintaining the same performance level. In [10], the advantages of using inerters when protecting buildings from earthquake excitation were examined. The research presented in [11,12] uses what they termed a tuned viscous mass damper, where an inerter is used as a mass amplifier. In [11], the effectiveness of the tuned viscous mass damper for seismic excitation is verified by testing a small-scale device on a shaking table.

Detailed models of an inerter have been developed in [13,14]. In [13], both flywheel and ball screw inerters were tested using standard hydraulic damper test rigs. Stability issues were encountered because of the lag between the real inerter force and that expected from an ideal damper. These were solved by connecting the inerter to a spring–damper buffer. With this adjustment, the combined device behaves as a damper around the crossover frequency and approaches ideal behaviour over a lower frequency range, friction being the major source of deviation from ideal. In [14], a ball screw inerter test was reported. Two major sources of nonlinear behaviour were identified: dry friction and nonlinear compliance. As in the previous study, it was found that friction was the major cause of deviance from ideal behaviour, together with stiffness effects. Backlash was not found to play a significant role in the dynamics of the inerter, because of pre-tensioning of the ball screw device. The impact of nonlinearities on vehicle suspension control systems was studied, concluding that performance was slightly degraded when compared with the equivalent linear system. Overall, the nonlinear inerter performs better than traditional non-inerter-based suspension systems. Other researchers studied the use of inerter-based compensators for controlling steering instabilities in motorcycles [15]. They reported the need to include parasitic inertances and damping in order to develop a complete model of the device [16,17].

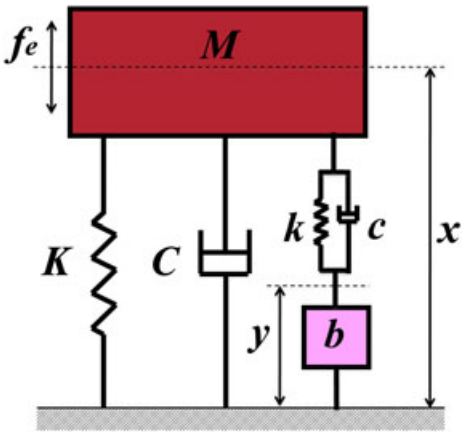

Figure 1. Host structural coupled with a mechanical tuned inerter damper.

DOI: 10.1002/stc

In civil engineering applications, the range of frequencies of interest is normally lower than in automotive engineering. For these low frequencies, the effects of nonlinearities are likely to be important and have a considerable impact on performance. Our research work focuses on two main issues: (i) what is the impact of the nonlinearities on the performance of the TID as a vibration suppressor and (ii) how to efficiently test inerter systems using real-time dynamic substructuring (RTDS). RTDS is a testing technique consisting of splitting the system being studied into substructures; some are represented numerically, and the others are physically built and tested. These substructures are made to interact in real time, so the response of the whole system can be studied.

A priori, the main advantage of using inerter-based vibration absorbers over traditional TMDs in civil engineering application is size. Size and weight are major constrains when designing vibration absorbers. Because of gearing, an inerter can amplify the inertial force associated with its weight by a considerable factor. For example, the commercially available inerter used in this work weighs 2 kg but the inertance is 75 kg. This is potentially very advantageous, for example, when developing absorbers for the new generation of tall buildings [18], where at the moment the major drawback with TMDs is their weight and size [19].

The paper is structured as follows. In Section 2, an ideal TID is presented and the parameters in the network are derived such that the performance is optimised, in terms of displacement of the host structure. In Section 3, the inerter is dynamically tested and an analytical model is derived. Section 4 studies numerically the optimisation problem including the nonlinear model developed in Section 3. Section 5 details the RTDS technique and the strategy developed to overcome the stability issues relating to the technique and hence allow testing of the inerter network. Section 6 presents the experimental results and studies the performance of the nonlinear TID as a vibration absorber. Conclusions are drawn in Section 7.

2. HOST STRUCTURE – IDEAL TUNED INERTER DAMPER

The TID device presented in [8], shown in Figure 1, is connected to a single-degree-of-freedom host structure. The force exerted by the TID onto the host structure, written in the Laplace domain, is given by

$$F_{TID} = \frac{cs + k}{bs^2 + cs + k} bs^2 X = -T_{TID} X \tag{1}$$

where k, c and b are the stiffness, damping and inertance of the TID, respectively, and X is the displacement of the host structure in the Laplace domain. Because a single-degree-of-freedom structure is considered, only one force is generated, and the other terminal of the inerter is being fixed.

In [8], the authors apply the fixed-points theory proposed by Den Hartog [20] to determine analytically the optimal TID damping ratio and TID-to-host structure frequency ratio. The derivation in [8] considered base-excited structures with the aim of minimising the host structure absolute displacement. However, the derivation results in a cubic equation, leading to the conclusion that for TIDs, there are three fixed points instead of two, as is the case for a TMD. Here, the application is changed, in the sense that we are looking at a structure where the forcing is applied on the host structure mass, rather than at the base. The parameter to be optimised is the displacement of the host structure, x. A sinusoidal concentrated force of the form $f_e(t) = Asin(\omega t)$ is considered, where A is the forcing amplitude. This is shown in Figure 1. For consistency with Den Hartog's derivation, the structural damping is ignored at this stage, $C = 0$.

The transfer function between the primary mass displacement, X, and the external force, F_e, can be written as

$$\frac{X}{F_e} = \frac{1}{Ms^2 + K - T_{TID}} \tag{2}$$

where T_{TID} can be obtained from Equation (1).

DOI: 10.1002/stc

Writing Equation (2) in the frequency domain results in

$$\frac{X}{F_e}(j\omega) = \frac{1}{-M\omega^2 + K - T_{TID}(j\omega)} \tag{3}$$

where $T_{TID}(j\omega) = -\frac{-b\omega^2(cj\omega+k)}{-b\omega^2+cj\omega+k}$, $j = \sqrt{-1}$ and F_e is the Laplace transform of the external force.

In order to evaluate the response amplitude, the real and imaginary terms can be regrouped, and Equation (3) is expressed in the form

$$\frac{X}{F_e}(j\omega) = \frac{A + Bj}{C + Dj} \quad , \quad \text{hence,} \quad \left|\frac{X}{F_e}\right|^2 = \frac{A^2 + B^2}{C^2 + D^2} \tag{4}$$

where $A = -b\omega^2 + k$, $B = c\omega$, $C = (-M\omega^2 + K)(-b\omega^2 + k) - bk\omega^2$ and $D = c\omega(K - M\omega^2 - b\omega^2)$. Replacing $b = \mu M$ and $k = \alpha\mu K$ and regrouping the terms as a function of c, we obtain

$$\left|\frac{X}{F_e}\right|^2 = \frac{(-\mu M\omega^2 + \alpha\mu K)^2 + \omega^2 c^2}{[(-M\omega^2 + K)(-\mu M\omega^2 + \alpha\mu K) - \alpha\mu^2 MK\omega^2]^2 + [(-M\omega^2 + K) - \mu M\omega^2]^2\omega^2 c^2} \tag{5}$$

where α is a scalar coefficient representing the squared frequency ratio between the TID and primary structure and $\mu = b/M$ represents the inertance-to-structural mass ratio, as defined before.

For consistence, we write

$$\left|\frac{X}{F_e}\right| = \sqrt{\frac{E + Fc^2}{G + Hc^2}} \tag{6}$$

where E, F, G and H can be found by comparing this equation with Equation (5).

As the initial objective is to find the coordinates of the fixed points, independent of the device damping, c, as in Den Hartog's derivation [20], the following condition must be enforced:

$$\frac{E}{G} = \frac{F}{H} \tag{7}$$

Substituting the expressions of E, F, G and H into Equation (7), using the notation $\overline{\omega}^2 = \frac{M}{K}\omega$ and square rooting, gives

$$\frac{-\mu\overline{\omega}^2 + \alpha\mu}{\left(-\overline{\omega}^2 + 1\right)\left(-\mu\overline{\omega}^2 + \alpha\mu\right) - \alpha\mu^2\overline{\omega}^2} = \pm\frac{1}{-\overline{\omega}^2 + 1 - \mu\overline{\omega}^2} \tag{8}$$

Considering the positive solution to Equation (8), after simple mathematical manipulation, the positive root becomes $\mu^2\overline{\omega}^4 = 0$, a trivial solution. The negative root may be simplified to a quadratic equation in $\overline{\omega}^2$

$$\overline{\omega}^4 - \frac{2(1 + \alpha + \alpha\mu)}{2 + \mu}\overline{\omega}^2 + \frac{2\alpha}{2 + \mu} = 0 \tag{9}$$

Equation (9) is identical to the equation obtained by Den Hartog [20] for TMDs. Therefore, it is not necessary to continue towards deriving the expressions of α and of the optimal damping ratio ξ, and we can use the results obtained by Den Hartog, namely,

$$\begin{cases} \alpha = \dfrac{1}{(1+\mu)^2} \\ \xi = \sqrt{\dfrac{3\mu}{8(1+\mu)}} \end{cases} \tag{10}$$

Being able to use the same tuning rules constitutes an advantage for the TID. However, as pointed out in [8], this is not the case for base displacement because the TID is connected both to the ground and the primary structure, while the TMD is only connected to the latter. Using Equation (10), the stiffness and damping parameters of the ideal (linear) TID can be calculated as

DOI: 10.1002/stc

$$\begin{cases} k = \mu\alpha \\ c = 2\xi\sqrt{kb} \end{cases} \tag{11}$$

The tuning methodology derived earlier can be summarised as follows:

Step 1 Choose the mass ratio, μ.
Step 2 Calculate the ratio between the squared TID and host structure fundamental frequencies, α and the damping ratio, ξ, using Equation (10).
Step 3 Calculate the optimal TID stiffness, k, and damping, c, using Equation (11).

However, this tuning methodology assumes the inerter is ideal, which, especially for low-frequency structures, is not necessarily a good assumption, as detailed in Section 1. A nonlinear model, based on experimental tests of the inerter considered in this paper, is proposed in the following section. The nonlinear model is then considered alongside the tuning rules used for its linear equivalent, to assess the deterioration in the performance of the TID due to its non-idealised behaviour.

3. INERTER DYNAMICS: EXPERIMENTAL RESULTS AND NUMERICAL APPROXIMATION

In this paper, a ball screw-type inerter manufactured by Penske, model PS8760H.218C, was tested. As a ball screw is difficult to seal, in the original design patented by the Penske group, a damper was built around the inerter by telescoping the ball screw directly into the damper shaft [21]. This allows the ball screw and thrust bearings to operate in the damper oil. In the tests presented here, most of the oil was extracted from the device, reducing the linear damping of the device to a negligible level, such that at low frequency, the device is not dominated by damping effects.

The behaviour of the tested inerter can be approximated by a nonlinear model, including dry friction in parallel with the inertance. A schematic representation of this model is shown in Figure 2(a), where b is the inertance and f_f is the dry friction. The value of the inertance, b, was supplied by the manufacturer, while the dry friction was evaluated by running low-frequency tests. For low frequencies, the measured force is dominated by the dry friction. Figure 2(b) shows an example sinusoidal cyclic displacement test conducted at 0.5 Hz. It is noted that the measured force, f_s, is almost a square wave, with an amplitude of 20 N and the sign matching that of the velocity across the inerter terminals, $\dot{y}$.

Both b and f_f values were verified for different sinusoidal inputs. Figure 3 shows the measured force, f_s, and the theoretical force, f_{th}, when the input to the inerter is a displacement sine wave at (a) 3 Hz and (b) 4 Hz, respectively. It can be seen from the experimental records, shown in Figure 3, that although there are some dynamics that are not captured by the simple nonlinear model, it does give a reasonable prediction of the behaviour of the inerter. The stiffness effect, backlash, linear damping and parasitic inertance could be included in a more complete model. However, this is unnecessary here as we wish

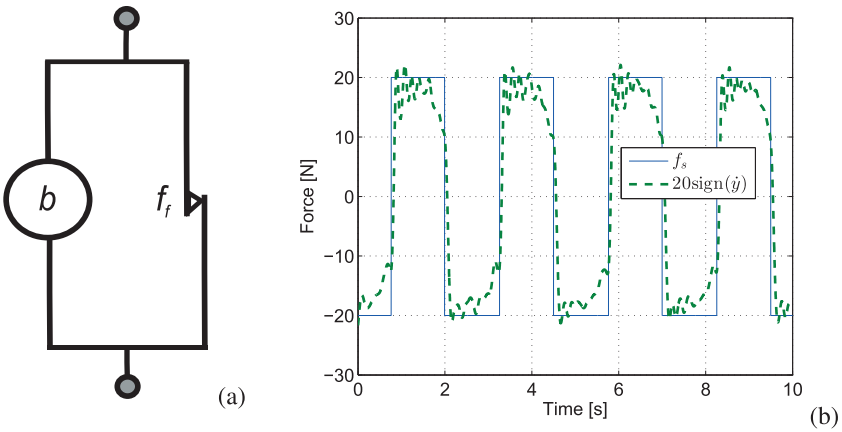

Figure 2. Inerter dynamics identification: (a) dynamics model and (b) estimating dry friction: experimental records for velocity, $\dot{y}$, and force, f_s. Low-frequency tests at 0.5 Hz.

DOI: 10.1002/stc

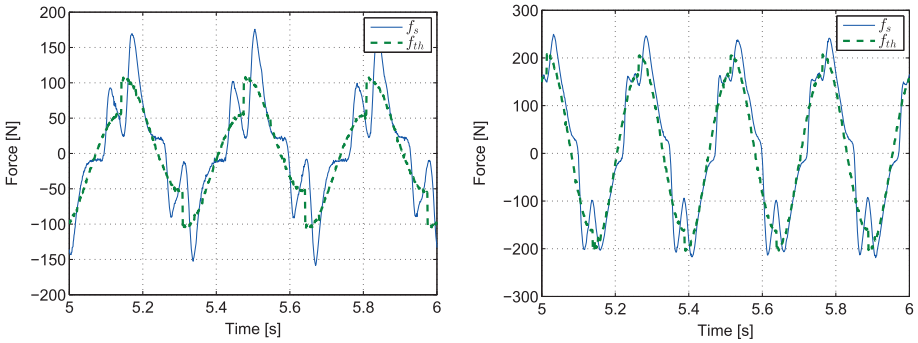

Figure 3. Verification of the analytical model. Theoretical and measured forces when (a) the input is a 3-mm displacement sine wave at 3 Hz and (b) the input is a 4-mm displacement sine wave at 4 Hz.

to understand the broad effect of the device dynamics on the tuning before assessing it experimentally using RTDS.

4. HOST STRUCTURE – NONLINEAR TUNED INERTER DAMPER COUPLING

In this section, we assess the effect of the inerter's nonlinear behaviour on the device tuning and subsequent performance, numerically. Starting from the identification work presented in Section 3, the parameters of the nonlinear TID are implemented in the numerical model in order to evaluate the effect of the real device's nonlinear behaviour on the performance. The new host structure with a nonlinear TID system is shown in Figure 4, and the equations of motion characterising the new structure are

$$\begin{cases} M\ddot{x} + C\dot{x} + Kx + c(\dot{x} - \dot{y}) + k(x - y) = f_e, \\ b\ddot{y} + c(\dot{y} - \dot{x}) + k(y - x) + f_f \text{sign}(\dot{y}) = 0 \end{cases} \tag{12}$$

We call f_e and f_f the external forcing and dry friction, respectively. Because of the presence of the signum function in the second equation, it is not favourable to use the Laplace domain as performed in [8]. Therefore, the equations will be solved numerically.

4.1. Parameters of the host structure and ideal tuned inerter damper

The fundamental frequency of the host structure is $\omega = 4$ Hz, and the mass is taken to be $M = 1500$ kg. Recalling that the inertance of the Penske inerter is $b = 75$ kg (from a 2-kg device), this gives a mass ratio of $\mu = 0.05$. Based on the mass and the fundamental frequency, the structural stiffness is $K = 947$ kN/m. In this analysis, the structural damping is reintroduced, with it set to 2 % or $C = 1.5$ kNs/m.

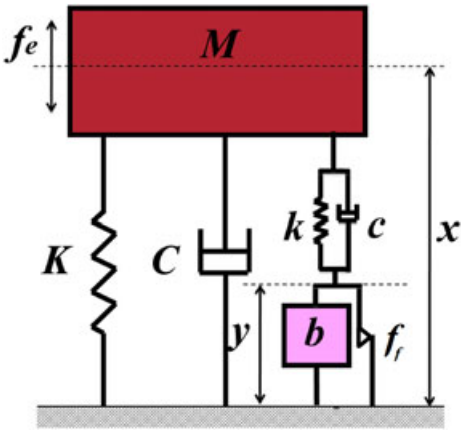

Figure 4. Host structure with a nonlinear tuned inerter damper device: numerical response for a range of forcing amplitudes.

DOI: 10.1002/stc

The parameters of the ideal (linear) TID are calculated using Equations (10) and (11) and following steps 1–3 presented in the previous section, leading to $\alpha = 0.907$ and $\xi = 0.134$. Using these values, it follows that $k = 42.97$ kN/m and $c = 0.479$ kNs/m.

4.2. Evaluation in the impact of the inerter nonlinearity

Recalling that the external force acting on the host structure has the form $f_e(t) = A\sin(\omega t)$, the forcing amplitude is varied to assess the impact of the TID nonlinearity for different excitation levels. The forcing amplitude spans from 100 to 1000 N, with increments of 100 N. Two larger values are then selected, namely, $A = 1500$ N and $A = 3000$ N, in order to observe the device's behaviour when the displacement is near the maximum stroke ($2y_{\max} = 14$ cm).

Figure 5(a) shows how the maximum normalised displacement of the host structure, x, varies with the forcing frequency. The thin solid lines represent the nonlinear system response for a variety of forcing amplitudes. At low amplitudes, the normalised displacement is larger and only one peak is present. When the amplitude increases, the curves tend to that of the linear TID (thick dashed line), as at high forcing levels, the effect of dry friction reduces in significance. The reduced performance at low amplitudes suggests that, if the device is expected to perform in this regime, it would be beneficial to retune the TID system by adjusting its stiffness and damping.

Figure 5(b) shows the inerter maximum normalised displacement, y, variation with the forcing frequency, for several forcing amplitudes. As with the case of the host structure displacement, the response becomes similar to that of the ideal TID as the forcing amplitude increases. However, now the normalised response amplitude increases with forcing amplitude. Also, it should be noted that for very low amplitudes, as $A = 100$ N and $A = 200$ N (the two lowest amplitude lines shown), the inerter can only be mobilised over a narrow frequency band. Note that this only appears in the numerical model and is not found in the experimental data (Section 6).

After evaluating the response of the nonlinear TID-controlled structure for a range of amplitudes, the device is retuned to optimise its performance, by minimising the displacement response of the host structure. With the nonlinear effect included, the split peaks shift, resulting in the fixed points having different amplitudes. Therefore, it is necessary to adjust the TID stiffness accordingly. Once the fixed points reach equal amplitudes, the TID damping is tuned such that the response curve has a horizontal tangent in the fixed points, following Den Hartog's guidelines [20].

Figure 6(a)–(c) shows the retuning iterations for $A = 200$ N, $A = 400$ N and $A = 600$ N, respectively. The stiffness has already been updated to obtained equal amplitude fixed points, and only the damping variation is shown. The normalised response using a linear TID is added in all panels for reference and is shown using the thick dashed line. In Figure 6(a), it can be seen that without retuning, the system response is dominated by the dry friction. There is only one resonant peak, occurring at a frequency situated close to the fundamental frequency of the host structure (shown using the thick

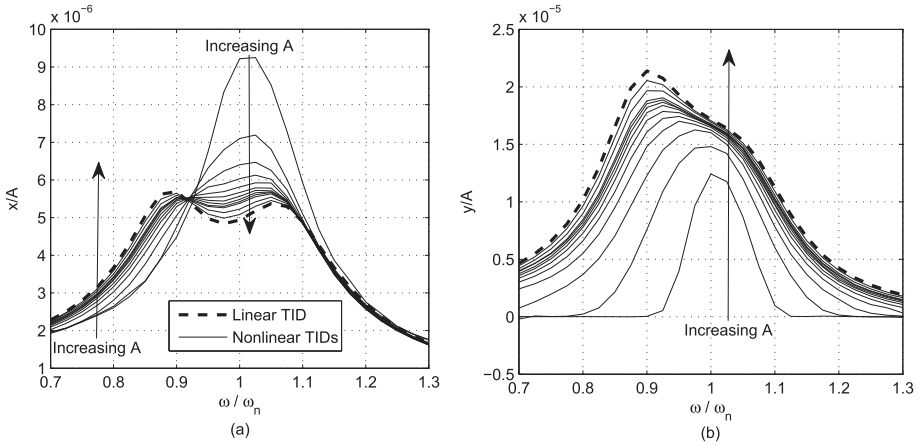

Figure 5. Frequency response of the structure equipped with a nonlinear tuned inerter damper (TID) device: (a) displacement of the main mass and (b) inerter displacement.

DOI: 10.1002/stc

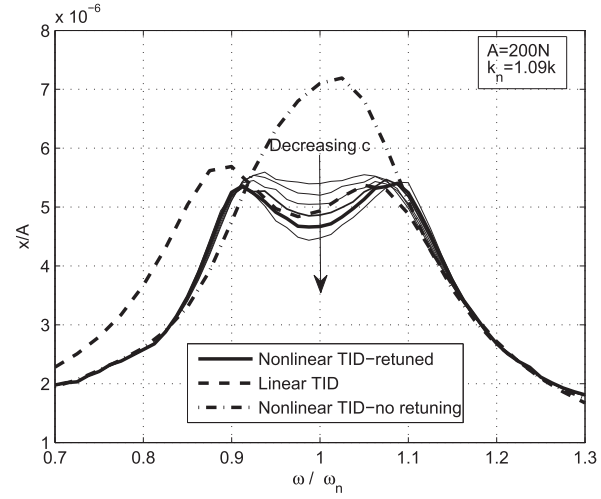

(a)

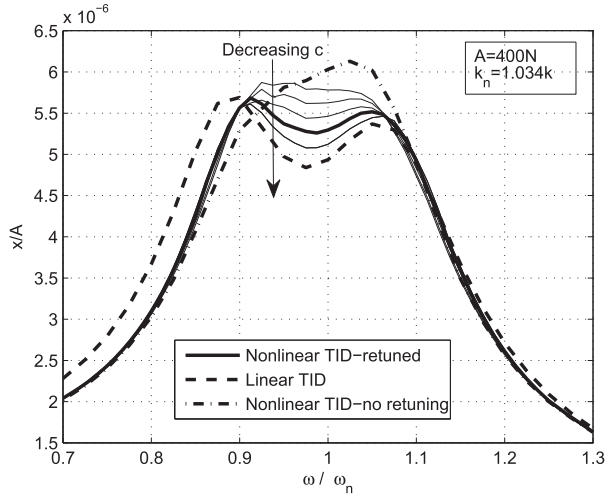

(b)

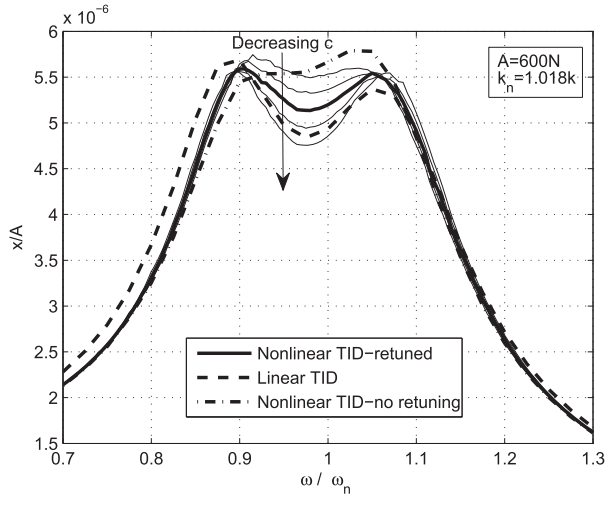

(c)

Figure 6. Retuning of the tuned inerter damper (TID) to accommodate nonlinear inerter effects by varying the damping once the stiffness has been adjusted to equalise the amplitude of the fixed points for (a) $A = 200$ N (with $k_n = 1.09k$); (b) $A = 400$ N (with $k_n = 1.034k$) and (c) $A = 600$ N (with $k_n = 1.018k$).

DOI: 10.1002/stc

dash-dotted line). By varying the TID parameters, it is found that the split peaks can be regained if the TID damping is lowered. The optimal stiffness of the nonlinear TID is $k_n = 1.09k$. After fixing k_n, the damping is varied and the curves obtained in each case are shown using the thin solid lines. The optimal response is obtained when the damping of the nonlinear TID is set to $c_n = 0.45c$ (thick solid line), compensating for the high effect of the dry friction. As can be seen, the optimal retuned nonlinear TID performance is very similar to that of the linear device. The same procedure was applied to retune the system for other forcing amplitudes shown in Figure 6(b) and (c). It is noted that as the forcing amplitude increases, the necessary increase in TID stiffness drops from 9 % to 3.4 % and then 1.8 % for forcing amplitudes of $A = 200$ N, $A = 400$ N and $A = 600$ N, respectively. For $A = 400$ N and $A = 600$ N, the decrease in required damping is not as dramatic, the new parameters being $c_n = 0.85c$ and $c_n = 0.9c$, respectively. In both cases, the retuned nonlinear system performance is very close to that of the linear TID. Moreover, as the forcing amplitude increases, the nonlinear TID performance, even without retuning, improves and the split peaks are present. This can also be concluded from the smaller changes necessary in the linear TID parameters.

The same retuning procedure was applied across the full amplitude range. The ratios between the updated stiffness and damping and the linear TID values are plotted in Figure 7(a) and (b), respectively. For low amplitudes, the TID stiffness must be increased up to 20 %, while damping drops to $0.18c$. For higher amplitudes, the retuned parameters are situated close to the ones of the linear TID. This means that retuning is only necessary for low-amplitude forcing. Also, the gradient of both curves is large for $A < 400$ N. Then, the retuned parameters ratio to the linearly tuned values slowly converges to 1, as A increases to 3000 N, where the maximum inerter stroke is reached.

The tuning methodology used for finding the optimal nonlinear TID parameters can be summarised as follows:

Step 1–3 The same as in the case of linear TIDs tuning.
Step 4 Evaluate the structural response for a range of TID stiffness and damping parameters situated in the vicinity of the initial guess represented by the parameters derived in step 3.
Step 5 Check the existence of fixed points and their new locations. These may not exist for low-amplitude forcing, where the nonlinearity has a stronger impact. If the fixed points exist, we proceed to applying steps 6 and 7.
Step 6 Adjust the value of k such that the fixed points have equal amplitudes.
Step 7 Adjust the value of c such that the tangent to the response curve, through the fixed points, is horizontal.

Finally, Figure 8(a) shows the variation of the host structure maximum displacement with the excitation amplitude. First, consider the effect of the nonlinearity by comparing the response of the ideal linear TID (dashed line) with the nonlinear TID (dash-dotted line) where both have been tuned

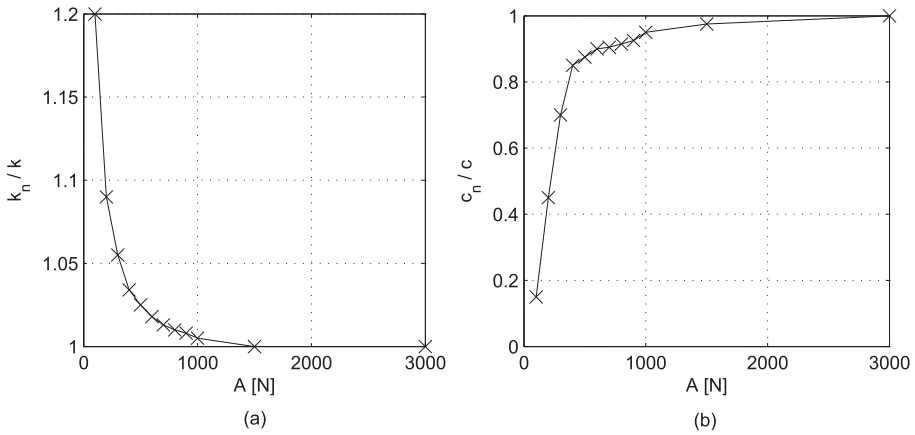

Figure 7. Variation of the device parameters with forcing amplitude: (a) normalised stiffness and (b) normalised damping, based on retuning.

Structural Control and Health Monitoring published by John Wiley & Sons, Ltd. DOI: 10.1002/stc

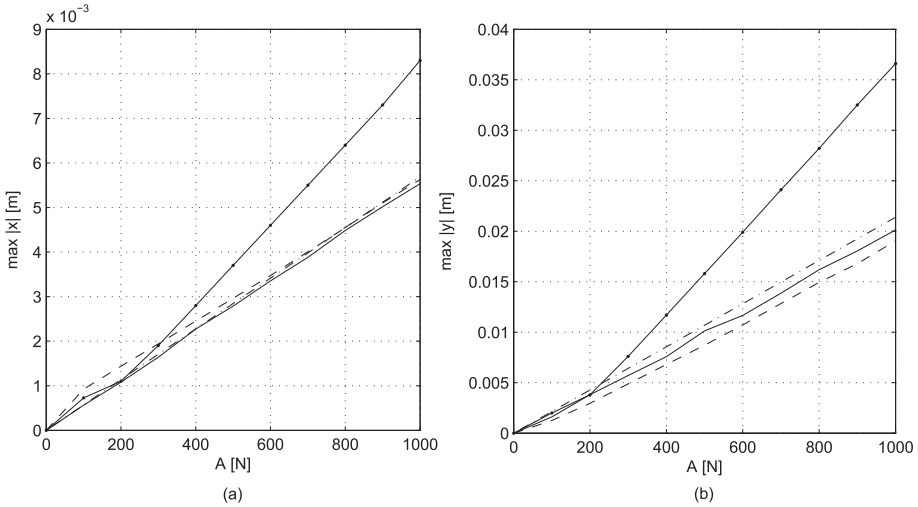

Figure 8. Variation of maximum displacement with forcing amplitude: (a) x and (b) y. The solid line represents the nonlinear tuned inerter damper (TID) retuned to account for the nonlinear effects for every forcing amplitude; the dashed line represents the nonlinear TID tuned as a linear TID; the dash-dotted line represents the linear TID; and the solid line with bullet markers represents the nonlinear TID, retuned for $A = 200$ N only.

assuming the device is linear. As can be seen, the difference between the curve corresponding to the nonlinear TID, where linear TID tuning has been used, and its linear equivalent is larger for lower amplitudes (50 % difference for $A = 100$ N) and then decreases until the curves almost coincide for $A > 600$ N. If the nonlinear device is retuned to account for the nonlinearity (solid line), the response is very close to that of the ideal linear device. A slight improvement can be observed where the solid line is situated below the dash-dotted line at high amplitudes.

All systems show good performance compared with the uncontrolled structure. Now, if the TID is tuned for an amplitude $A = 200$ N and then forced at higher amplitude, its performance deteriorates significantly (solid line with bullet markers), the maximum displacement being approximately 50 % higher than the one corresponding to the nonlinear TID without retuning, when $A = 1000$ N. Panel (b) shows the same results but in terms of inerter maximum displacement, y. In this case, the linear TID leads to the highest displacement, while the nonlinear TID shows the smallest values. Therefore, no retuning is necessary to control the inerter displacement. However, in the retuning process, y increases slightly, the solid line being approximately the average of the dashed and dash-dotted lines. Also, a significant increase in the inerter displacement is noted when the device is retuned for low-amplitude excitation but forced at a higher amplitude.

It is concluded that the retuning has a high impact on the structural performance at low amplitudes only, where the response is dominated by dry friction. However, structural displacements are low here so retuning would arguably only be needed for comfort rather than structural performance. At high amplitudes, where the inertial nature of the inerter prevails, retuning is not necessary. Moreover, the TID should not be retuned for low amplitudes unless we are sure it will not be subject to higher amplitude excitation. Otherwise, the host structure and TID displacement increase significantly when subjected to the higher amplitude excitation, so the retuning could potentially lead to the failure of the elements.

5. STABILITY OF THE SUBSTRUCTURING TESTS

Real-time dynamic substructuring is a testing technique developed to overcome limitations of more traditional methods, such as shaking table testing (scaling issues) and pseudodynamic testing (damping effects lost). The idea is to split the system being considered into two subsystems, one numerical and one physical, allowing full-scale and real-time testing of a crucial element within the system [22]. These two subsystems interact in real time via actuators and sensors with the objective of achieving compatibility and equilibrium at the interface in real time. If this objective is met, the subsystems

DOI: 10.1002/stc

will emulate the full system in real time. RTDS testing is effective when the nonlinearities or unmodelled dynamics of a system are concentrated or when new components need to be tested within the context of a whole assembly.

When developing RTDS tests, one has to consider the numerical and physical degrees of freedom that interact in real time [22]. Stability problems can arise if the control at the interface is not ideal, which is not uncommon, because of the interface actuator dynamics. The performance of RTDS is often assessed by studying the effect of displacement delay at the interface. Details on the modelling of substructuring testing using delay differential equations can be found in [23–25]. To present the techniques, let us consider a reference example to clarify where the delay comes from and its effects in the experiment stability; see details of this example in [23]. The structure depicted in Figure 9 is the reference model. The whole system is divided into two subsystems: a numerical one including m, c and k_1 and a physical one, k_2. We study the response of the system under external forcing, f_e. The numerical model will calculate a displacement at the interface, x, under forcing, f_e. This displacement is applied to the physical spring by a transfer system, normally an actuator. This actuator, and its associated controller, introduces unwanted dynamics into the system, which are often modelled as a delay, τ, which is usually in the range of tens of milliseconds [23]. The force generated at the interface due to the applied displacement is measured, normally via load cells, and fed back into the numerical model. The numerical model calculates a new displacement considering an input force, $f_e - f_s$. This loop, represented in Figure 9, is repeated in real time until the end of the test. The experiment will be stable if the numerical model is stable. For this simple example, the equation being solved is $m\ddot{x}(t) + c\dot{x}(t) + k_1 x(t) + k_2 x(t-\tau) = f_e(t)$. The stability of this equation depends on τ, and it can be studied using ordinary delayed differential equation theory. Note that techniques to reduce to a minimum the effects of delay are always applied in RTDS, based on forward prediction [22], but it is impossible to completely negate the effect of actuator-induced delay.

The problem becomes more challenging when the delays are in acceleration terms. This is the case when some of the mass is in the physical substructure (Figure 10). In this case, the feedback force $f_s(t) = m_2\ddot{x}(t-\tau)$ and the equation to solve is given by $m_1\ddot{x}(t) + m_2\ddot{x}(t-\tau) + c\dot{x}(t) + kx(t) = f_e(t)$, a neutral delayed differential equation, and the stability margins are much smaller than in the previous case, when dealing with ordinary differential equations [24,25]. In the extreme, if a degree of freedom is split such that the mass is physical but stiffness and damping are numerical, Figure 10, $f_s(t) = m\ddot{x}(t-\tau)$ and the equation to solve is given by $m\ddot{x}(t-\tau) + c\dot{x}(t) + kx(t) = f_e(t)$. This is an advanced equation, and the experiment will be strongly unstable for any delay value. This last case is highly relevant to the inerter testing. To explain why it is called an advanced equation, consider the simple advanced equation, borrowed from [26]: $\dot{x}(t) = \ddot{x}(t-\tau)$; by a τ-shift transformation in time, and by using the new variable $z(t) = \dot{x}(t)$, the equation can be rewritten in the form $\dot{z}(t) = z(t+\tau)$. Here, the rate of the change of state is determined by the future values of the state. While linear autonomous delayed differential equations have infinitely many poles on the left half of the complex plane, linear autonomous advanced differential equations have infinitely many poles on the right half of the complex plane. In this sense, they are always strongly or infinitely unstable [26].

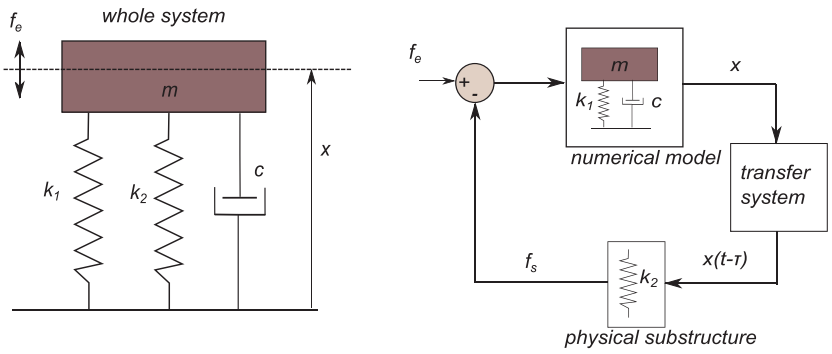

Figure 9. Example of a reference emulated system and its associated substructuring loop.

DOI: 10.1002/stc

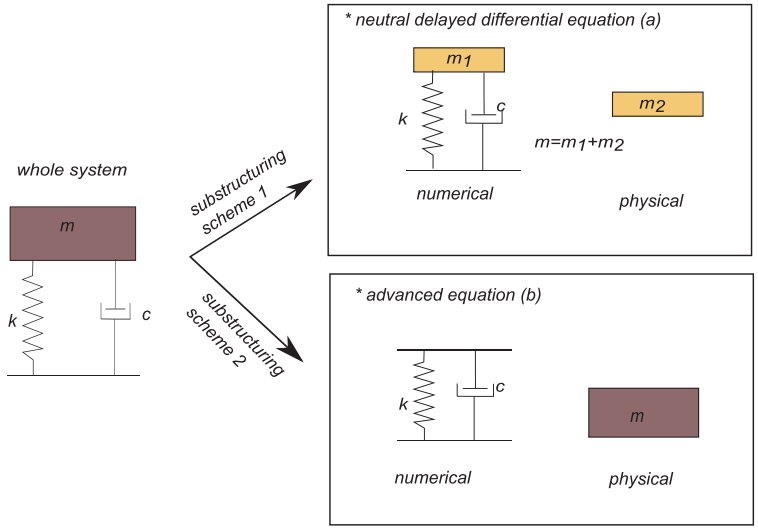

Figure 10. Splitting a degree of freedom: (a) the numerical model to solve will be a neutral delayed differential equation and (b) the numerical model to solve will be an advanced equation.

Our substructuring configuration divides the system into two substructures: the numerical one contains the host structure and the spring k and damper c of the TID; the physical substructure is represented by the inerter device (Figure 11). The idea behind this configuration is to have freedom to change the values of k and c so the TID system is optimal, without making physical alterations to the experimental setup. For this study, this split is optimal because (i) we are able to change the values of k and c in our experiment very easily (as they are numerical) and find optimal values and (ii) we are able to study the effect on performance of nonlinearities in the inerter, as the inerter physically tested. The accuracy of the RTDS testing has been studied in [24], where a highly nonlinear system was considered. It was concluded that it is accurate to model nonlinear systems using the technique, provided accurate displacement control at the interface.

To link the two substructures, an actuator is used to impose displacement y on the inerter, and the force required to do this, f_s, is measured by a load cell and fed back to the numerical model. Because of the dynamics of the actuator, the actual displacement imposed to the physical substructure, y^*, is considered delayed by τ seconds, such that $y^*(t) = y(t-\tau)$. The dynamics of the numerical substructure are defined by

$$\begin{aligned} M\ddot{x}(t) + C\dot{x}(t) + Kx(t) &= f_e(t) - f_s(t) \\ f_s(t) &= c(\dot{x}(t) - \dot{y}(t)) + k(x(t) - y(t)) \end{aligned} \tag{13}$$

where f_e is the external forcing and f_s is the force at the interface or substructuring force.

Considering an ideal inerter, the measured force at the interface will be $f_s = b\ddot{y}^*(t) = b\ddot{y}(t-\tau)$.

Combining these two equations, the resulting equation is an advanced equation, as the previously defined example, and is highly unstable [26]:

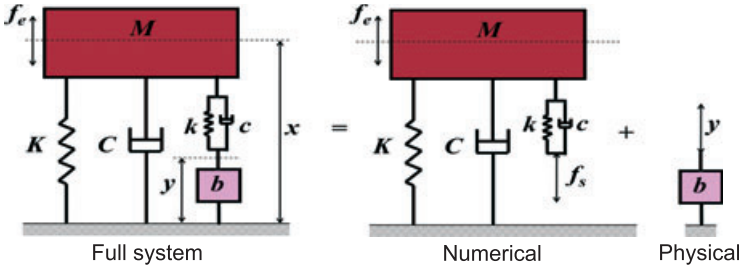

Figure 11. Substructuring configuration scheme. Physical substructure: the inerter; numerical substructure: the host structure and the spring and damper of the tuned inerter damper.

DOI: 10.1002/stc

$$b\ddot{y}(t-\tau) + c(\dot{y}(t) - \dot{x}(t)) + k(y(t) - x(t)) = 0 \tag{14}$$

Taking the Laplace transform of Equation (13), we obtain

$$\begin{aligned} X(s) &= \frac{F_e(s) - F_s(s)}{Ms^2 + Cs + K}; \\ Y(s) &= \frac{Ms^2 + (C+c)s + (K+k)}{cs+k}X(s) - \frac{1}{cs+k}F_e(s) \end{aligned} \tag{15}$$

Using the Laplace equation derived earlier, the substructured system can be represented by the feedback loop presented in Figure 12. It can be seen that the closed loop for $F_e = 0$ has four zeros and three poles, resulting in a non-causal problem. It is not possible to implement this setup with any delay present, even in a pure numerical simulation.

In order to be able to implement the substructuring configuration, we redefine the problem by assuming an interface force, based on a *guessed* inertance, b_g, such that $f_{sth}(t) = b_g\ddot{y}(t)$. Using this, the signal fed back to the numerical model, the second line of Equation (15) will represent the error between the assumed interface force and the actual force measured at the interface, f_s. The fed back error will account for linear and nonlinear effects not captured in $f_{sth}(t) = b_g\ddot{y}(t)$. The new equations are therefore

$$\begin{aligned} M\ddot{x}(t) + C\dot{x}(t) + Kx(t) &= f_e(t) - f_s(t) \\ b_g\ddot{y}(t) + c(\dot{y}(t) - \dot{x}(t)) + k(y(t) - x(t)) &= -e(t) \end{aligned} \tag{16}$$

where $e(t) = f_s(t) - b_g\ddot{y}(t)$. Taking the Laplace of Equation (16) transform, we obtain

$$\begin{aligned} X(s) &= \frac{F_e(s) - F_s(s)}{Ms^2 + Cs + K}; \\ Y(s) &= \frac{(cs+k)}{b_g s^2 + cs + k}X(s) - \frac{E(s)}{b_g s^2 + cs + k} \end{aligned} \tag{17}$$

The closed loop of the redefined problem is shown in Figure 13. Note that for the RTDS tests, the inerter transfer function is replaced by the physical device.

The key feature of this setup is that it requires a crude model of the inerter dynamics, with an error feedback to mitigate the effects of the crude model. Let us assume that the actual inertance is b, and there is some unknown linear dynamics with Laplace transform equal to $U(s)y$. The dynamics of the whole system can be defined by the following transfer functions:

$$\begin{aligned} X(s) &= \frac{F_e(s) - (bs^2 + U(s)Y(s))}{Ms^2 + Cs + K} \\ Y(s) &= \frac{(cs+k)}{bs^2 + cs + k + U(s)}X(s) \end{aligned} \tag{18}$$

In the substructured system, if we take $Y^*(s) = Y(s)$, such that ideal control is achieved [23], the

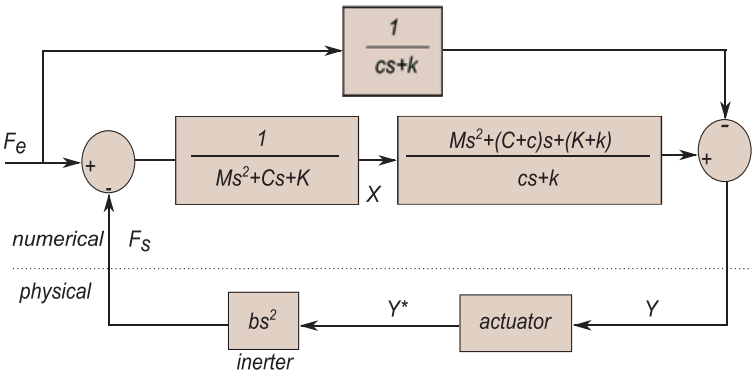

Figure 12. Substructuring configuration loop. Physical substructure: the inerter; numerical substructure: the host structure and the spring and damper of the tuned inerter damper.

DOI: 10.1002/stc

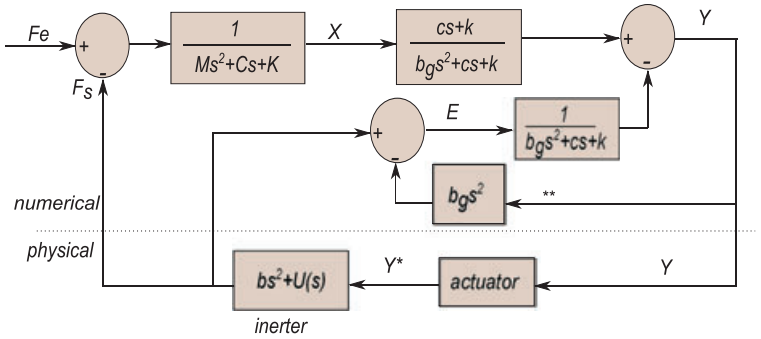

Figure 13. Improved stability substructure configuration. Physical substructure: the inerter; numerical substructure: the host structure, the spring and damper of the tuned inerter damper and the inerter with *guessed* inertance, b_g.

measured force at the interface is $F(s)=(bs^2+U(s))Y(s)$, and the error is defined by $E(s)=((b-b_g)s^2+U(s))Y(s)$. By substituting $X(s)$ into $Y(s)$ in Equation (17), we obtain

$$Y(s)=\frac{(cs+k)F_e(s)}{(Ms^2+Cs+K)(bs^2+U(s)+cs+k)+(bs^2+U(s))(cs+k)} \tag{19}$$

where all terms containing b_g vanish. This expression is the same as that obtained if we substitute $X(s)$ into $Y(s)$ in Equation (18), corresponding to the entire system, thus demonstrating that the substructured system reproduces the dynamics of the full emulated system when the control at the interface is accurate.

The dynamics of physical substructures are likely to exhibit nonlinearity, such as the dry friction in the inerter, and it could be the case that it is not possible to define $U(s)$. In order to study the effectiveness of this technique in the presence of a nonlinearity, a numerical model using Simulink was developed, considering the inerter model shown in Figure 2, which includes dry friction in parallel with the inertance. The results from the simulated susbtructuring configuration were compared with the results from simulating the whole system, obtaining a very good agreement. It was also found that the accuracy of the results was not very sensitive to the value we assign for the *guessed* inertance b_g. Figure 14 compares the numerical results of the whole system and the substructured system. Displacement of both host structure and TID is shown in this figure. The x and y displacements are plotted for two simulations: whole system (dashed line) and substructures system using the proposed technique (points). In the example gathered in Figure 14, where $b_g=0.8b$ was chosen, the very good agreement for both x and y can be seen. Note that in the substructuring test, and in the numerical simulation of the test, the term b_gs^2y (labelled ** in Figure 13) is approximated by $-b_g\omega^2y$, where ω is the frequency of

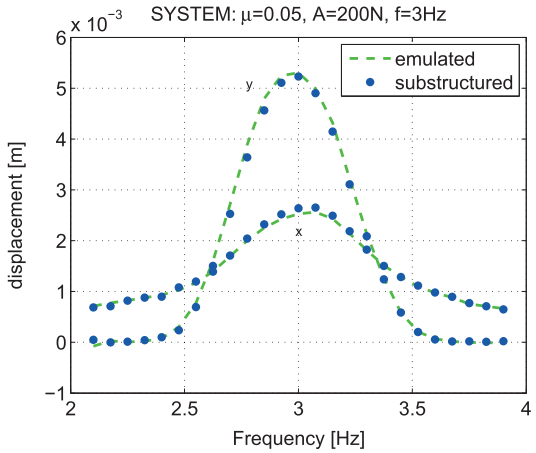

Figure 14. Substructuring simulation results compared with those from the full emulated system for the case where $b_g=0.8b$; dashed line, whole system; bullet markers, substructured system.

DOI: 10.1002/stc

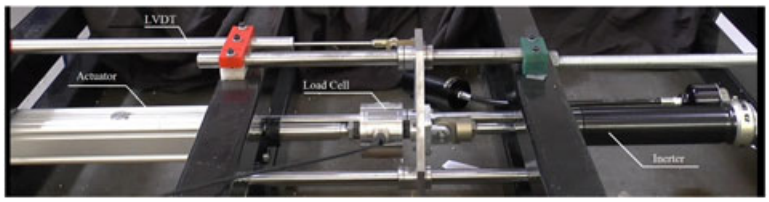

Figure 15. Picture of the experimental setup.

the external force, to avoid numerical double differentiation errors. By doing this, some high harmonic content of the signal is lost, but the results are reasonably accurate, as shown in Figure 14.

Previous research on stabilising RTDS tests has dealt with delay differential equations (that is, stiffness or damping in the physical substructure) [23,27] or neutral differential equations (a mass split where more than half of the total mass is numerical interfacing with less than half mass on the physical side) [25,27] but not advanced ones, as reported here.

The simulation results suggest that the proposed strategy is accurate. This is in contrast to the conventional system represented in Figure 12, where it was not even possible to simulate because of its unstability.

By redefining the problem in terms of the inertance estimation error, $e(t)$, we have transformed an advanced equation, Equation (14), into the following neutral differential equation:

$$\begin{aligned} b_g\ddot{y}(t) + e(t) + c(\dot{y}(t) - \dot{x}(t)) + k(y(t) - x(t)) = 0; \\ e(t) = f(y(t-\tau), \dot{y}(t-\tau), \ddot{y}(t-\tau)) \end{aligned} \tag{20}$$

For details on stability of neutral differential equations in the context of RTDS, see the work of Kyrychko *et al.* [25].

6. SUBSTRUCTURING EXPERIMENTAL RESULTS

The inerter was mounted horizontally on a heavy bench. One terminal was clamped to the frame, while the displacement at the interface, y, was applied by an electromechanical actuator (Figure 15). This displacement at the interface is monitored using a Linear Variable Displacement Transducer (LVDT) and the force is measured by a load cell. Delay from the transfer system, the actuator, is compensated for by using a forward prediction technique [23]. The experiment was run in real time using Simulink and DSpace board. The numerical model is simulated using MATLAB Simulink. DSpace allows for real-time communication between the numerical model and the physical substructure.

Figure 16 contains a set of experimental results. They correspond to low forcing, $A = 200$ N, when the nonlinearities affect more the behaviour of the device. The parameters are as follows: $b_g = 75$ kg,

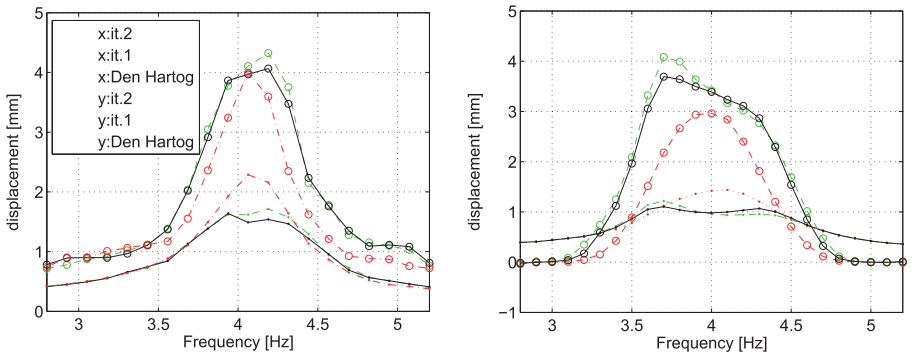

Figure 16. External force with $A = 200$ N. Points markers correspond to the host structure displacement, x; circle markers correspond to the inerter displacement, y. Tuning using Den Hartog (red), retuned iteration 1 (black) and iteration 2 (green); (a) experimental results and (b) analytical results using inerter model discussed in Section 2.

DOI: 10.1002/stc

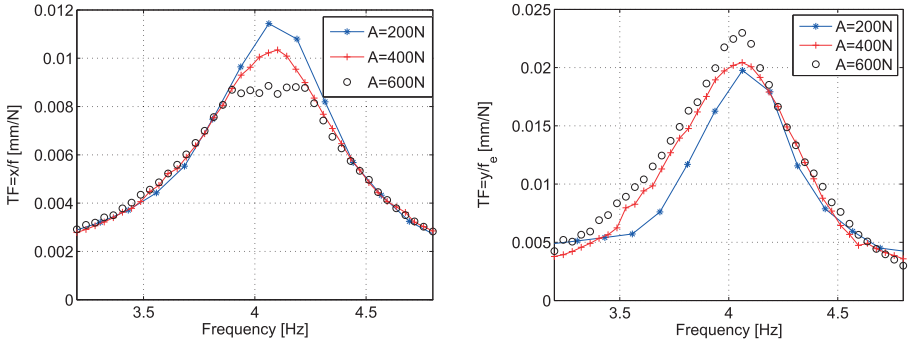

Figure 17. Transfer function: displacement/force. Experimental results for increasing levels of forcing. Asterisk markers correspond to $A=200$ N, crosses to $A=400$ N and circles to $A=600$ N; (a) host structure x/f_e and (b) tuned inerter damper y/f_e.

$\mu=0.05$, $M=1500$ kg, $K=9.5\times10^5$ N/m, $f=4$ Hz and $\zeta=0.02$, where f and ζ are the resonant frequency and damping ratio of the host structure. The parameters k and c of the TID, for the starting point, are chosen as the optimal values derived in Section 2 (equivalent to Den Hartog [20]), using α and ξ (Equation (10)).

Iteration 1 (it.1) corresponds to increasing k by 10 % and reducing c by 50 %. The values for the iteration were taken from the values derived from the numerical study and gathered in Figure 7. Iteration 2 (it.2) corresponds to increasing k by 15 % for more adjustment. Experimental results are qualitatively close to the numerical ones based on the simple nonlinear inerter model: the stiffness k has to be increased and damping c has to be decreased in order to retune the device. The experimental displacements are higher than the numerical ones; note that we are plotting the maximum peak displacements. This is thought to be due to the inerter compliance, which is not included in the nonlinear inerter model used to generate the numerical results.

As predicted by the numerical study developed in Section 4, for higher levels of excitation, the displacement of the inerter increases in relative terms, together with the bandwidth, and the device behaves closer to a linear one. The bandwidth does not increase as much as predicted numerically because of the nonlinear effects not captured by the analytical model used in the simulation section, such as backlash and stiffness effect. Figure 17 presents the transfer function of the displacement of the host structure, x, and the inerter, y, for increasing levels of excitation, from $A=200$ N to $A=600$ N, the maximum that could be applied with our experimental setup. Note that in this case, the k and c values were derived from Den Hartog's Equation (10).

7. CONCLUSIONS

In this paper, the performance of a TID used as a vibration absorber was studied analytically and experimentally. In the study, nonlinearities are included to study their effect on the TID performance. It was shown that the optimisation of a linear TID when the external forcing is acting on the host structure mass is equivalent to that of TMDs, proposed by Den Hartog. Following the inclusion of dry friction as a nonlinear parameter, it was concluded that the retuning of the linear TID is only necessary for low-amplitude loading scenarios, as the behaviour of the device converges to the ideal one for higher loads. However, retuning the TID to obtain optimal performance under low loading is detrimental if the host structure then experiences higher amplitude forcing, while the reciprocal is not as critical. Just a slight increase of the stiffness, in the order of 5 %, and decrease of the damping, 10 %, should be sufficient to assure a good performance of the device. The numerical findings were confirmed experimentally. The proposed network was tested using RTDS. Because of the experimental configuration, which allows changes in the stiffness and damping of the TID, the substructuring experiment was unstable when using the standard RTDS approach. A new approach for developing RTDS tests has been presented in order to overcome the instability due to delayed inertial forces. The results of the testing

DOI: 10.1002/stc

demonstrate the ability of the TID to absorb vibration from a host structure and backed up the numerical findings in qualitative terms. In brief, we can conclude that, for the commercially available inerter we considered, although the nonlinearities affect the behaviour of the TID, their effect is not dramatic, and in consequence, designing devices following Den Hartog's optimisation results in near-optimal performance.

REFERENCES

1. Smith MC. Synthesis of mechanical networks: the inerter. *IEEE Transactions on Automatic Control* 2002; **47**:1648–1662.
2. Swift SJ, Smith MC, Glover AR, Papageorgiou C, Gartner B, Houghton NE. Design and modelling of a fluid inerter. *International Journal of Control* 2013; **86**(11):2035–2051.
3. Brzeski P, Kapitaniak T, Perlikowski P. Novel type of tuned mass damper with inerter which enables changes of inertance. *Journal of Sound and Vibration* 2015; **349**:56–66.
4. Gonzalez-Buelga A, Clare LR, Neild SA, Jiang JZ, Inman DJ. An electromagnetic inerter-based vibration suppression device. *Smart Materials and Structures* 2015; **24**:055–015.
5. Smith MC, Wang FC. Performance benefits in passive vehicle suspensions employing inerters. *Vehicle System Dynamics* 2004; **42**(4):235–257.
6. Jian JZ, Matamoros-Sanchez AZ, Zolotas A, Goodall RM, Smith MC. Passive suspensions for ride quality improvement of two-axle railway vehicles. *Proceedings of the Intitution of Mechanical Engineers, Part F: Journal Rail and Rapid Transit* 2013; **0**(0):1–15.
7. Wang FC, Hsieh MR, Chen HJ. Stability and performance analysis of a full-train system with inerters. *Vehicle System Dynamics* 2012; **50**(4):545–571.
8. Lazar IF, Neild SA, Wagg DJ. Using an inerter-based device for structural vibration suppression. *Earthquake Engineering and Structural Dynamics* 2014; **43**(8):1129–1147.
9. Marian L, Giaralis A. Optimal design of a novel tuned mass-damper–inerter (TMDI) passive vibration control configuration for stochastically support-excited structural systems. *Probabilistic Engineering Mechanics* 2014; **38**:156–164.
10. Takewaki I, Murakami S, Yoshitomi S, Tsuji M. Fundamental mechanism of earthquake response reduction in building structures with inertial dampers. *Structural Control and Health Monitoring* 2012; **19**(6):590–608.
11. Ikago K, Saito K, Inoue N. Seismic control of single-degree-of-freedom structure using tuned viscous mass damper. *Earthquake Engineering and Structural Dynamics* 2012; **41**:453–474.
12. Sugimura Y, Goto W, Tanizawa H, Saito K, Nimomiya T. Response control effect of steel building structure using tuned viscous mass damper. *15th World Conference on Earthquake Engineering* 2012.
13. Papageorgiou C, Houghton NE, Smith MC. Experimental testing and analysis of inerter devices. *Journal of Dynamic Systems, Measurement, and Control* 2009; **131**:011001-1.
14. Wang FC, Su WJ. Impact of inerter nonlinearities on vehicle suspension control. *Vehicle System Dynamics: International Journal of Vehicle Mechanics and Mobility* 2008; **46**(7):575–595.
15. Evangelou S, Limebeer DJN, Sharp RS, Smith MC. Control of motorcycle steering instabilities. *IEEE Control Systems Magazine* 2006; **26**(5):78–88.
16. Papageorgiou C, Lockwood OG, Houghton NE, Smith MC. Experimental testing and modelling of a passive mechanical steering compensator for high-performance motorcycles. *Proceedings of the European Control Conference* 2007.
17. Jiang JZ, Smith MC, Houghton NE. Experimental testing and modelling of a mechanical steering compensator *ISCCSP*, *Malta*, 2008.
18. He YC, Li Q. Dynamic responses of a 492-m-high tall building with active tunedmass damping system during a typhoon. *Structural Control and Health Monitoring* 2014; **21**:705–720.
19. Li QS, Zhi LH, Tuan AY, Kao CS, Su SC, Wu CF. Dynamic behavior of Taipei 101 tower: field measurement and numerical analysis. *Journal of Structural Engineering* 2011; **137**(1):143–155.
20. Den Hartog JP. Mechanical Vibrations. McGraw-Hill: New York, 1947.
21. Shocks to the system. Racecar engineering, 2001. www.racevarengineering.com
22. Williams MS, Blakeborough A. Laboratory testing of structures under dynamic loads: an introductory review. *Philosophical Transactions of the Royal Society A* 2001; **359**:1651–1669.
23. Wallace MI, Sieber J, Neild SA, Wagg DJ, Krauskopf B. Stability analysis of real-time dynamic substructuring using delay differential equation models. *Earthquake Engineering & Structural Dynamics* 2005; **34**(15):1817–1832.
24. Gonzalez-Buelga A, Wagg DJ, Neild SA. Parametric variation of a coupled pendulum–oscillator system using real-time dynamic substructuring. *Structural Control and Health Monitoring* 2007; **14**(7):991–1012.
25. Kyrychko YN, Blyuss KB, Gonzalez-Buelga A, Hogan SJ, Wagg DJ. Real-time dynamic substructuring in a coupled oscillator–pendulum system. *Proceedings of the Royal Society A* 2006; **462**:1271–1294.
26. Insperger T, Stepan G, Turi J. Delayed feedback of sampled higher derivatives. *Philosophical Transactions of the Royal Society A* 2010; **368**:469–482.
27. Gawthrop PJ, Wallace MI, Neild SA, Wagg DJ. Robust real-time substructuring techniques for under-damped systems. *Structural Control and Health Monitoring* 2007; **14**(4):591–608.